Environmental Science Nano

The fate of CdS Quantum Dots in plants as revealed by Extended X-ray Absorption Fine Structure (EXAFS) analysis

Journal:	*Environmental Science: Nano*
Manuscript ID	EN-ART-12-2019-001433.R1
Article Type:	Paper

Environmental significance

The fate of Cd inside A. thaliana plant cells was studied using EXAFS spectroscopy applied to plants exposed to CdS QDs or CdSO4. It was found that the most likely mechanism for Cd incorporation involves the binding of Cd atoms by multiple type of molecules, resulting in slightly different local environments according the type of growth substrate (CdS QDs or $CdSO_4$). Moreover, we show that the QDs structure is only partially degraded, with Cd preserving some of its bonds with sulphur, thus indicating a reduced mobility and bioavailability of Cd following the uptake. In view of this, the presented results may be employed to investigate opportunities in terms of bio and phytoremediation. We provide for the first time a hypothesis on the response mechanisms of plants to CdS QDs from exposure to complete detoxification. This approach, unveiling the bio-transformation mechanisms occurring during Cd uptake by the plants, may as well provide crucial information on the behaviour and toxicity of CdS QDs in plants of greater importance for environment and agriculture.

The fate of CdS Quantum Dots in plants as revealed by Extended X-ray Absorption Fine Structure (EXAFS) analysis

Marta Marmiroli [1]§*, Giovanni Orazio Lepore [2]§*, Luca Pagano[1], Francesco d'Acapito[2], Alessandra Gianoncelli[3], Marco Villani[4], Laura Lazzarini[4], Jason C. White[5], Nelson Marmiroli[1,6]

1- Dept. Chemistry, Life Science and Environmental sustainability, University of Parma, Parma, Italy.

2- CNR-IOM-OGG c/o ESRF – The European Synchrotron, 71 Avenue des Martyrs CS 40220 F-38043 Grenoble Cédex 9, France.

3- Elettra - Sincrotrone Trieste, Strada Statale 14 - km 163,5 in AREA Science Park, Trieste, Italy.

4- IMEM-CNR, Parco Area delle Scienze, 34, Parma, Italy.

5- The Connecticut Agricultural Experiment Station, New Haven, CT, USA.

6- Consorzio Interuniversitario Nazionale per le Scienze Ambientali (CINSA), University of Parma, 43123 Parma, Italy.

§: the authors contributed equally to the work.

**: corresponding authors.*

Abstract

Use of Quantum Dots (QDs) is widespread and as such, the potential risk associated with their dispersion in the environment has stimulated research on interaction with potential sensitive receptors. To this end, the model plant *Arabidopsis thaliana* wild type (wt) and two mutant lines known to be tolerant to cadmium-based CdS QDs but not $CdSO_4$ were exposed to CdS QDs or $CdSO_4$ at sub-inhibitory concentrations for 20 days. X-ray Absorption Spectroscopy (XAS) was employed to investigate cadmium speciation in the cellular environment of the plants after treatment. After exposure to CdS QDs and $CdSO_4$, differences in biomass were observed between wt and mutants, but the form of Cd in the treatment had a marked influence on cadmium atomic environment. The spectra of whole plant samples were found compatible with a mixed O/S coordination: while Cd-S distances did not show ample variations, Cd-O distances varied from ≈2.16 Å in samples grown with QDs to ≈2.22 Å in those grown on $CdSO_4$. In addition, the amount of Cd-S bonds in plants grown with QDs was higher than Cd-O bonds. XAS data showed that CdS QDs were bio-transformed after their uptake; the particle original structure was modified but not totally eliminated, Cd atoms were not released as Cd (II) ions. These findings show the nanoscale specific response of plants to QDs, provide important insight to understanding nanoparticle fate in plants and in the environment, and have implications for both risk assessment and design of appropriate remediation strategies.

Keywords: X-ray Absorption Spectroscopy, biotransformation, molecular mechanisms, CdS QDs, *Arabidopsis thaliana*

Introduction

Engineered nanomaterials (ENMs) are substances that have particle dimensions in the range of 1–100 nm and at this scale, the ratio between the surface area and volume yields higher reactivity in comparison to the bulk material. Many ENMs exhibit unique physico-chemical properties, including optics, magnetics, dielectrics, density and mechanic resistance; therefore, these materials have found widespread use in different disciplines such as electronics, biomedicine, pharmaceuticals, cosmetics, environmental analysis and remediation, catalysis and material sciences.[1] Their projected market size of nanotechnology has been estimated at 55 billion USD by 2022.[2]

Cadmium sulfide-based quantum dots (CdS QDs) possessing the hexagonal crystal structure of wurtzite (ZnS) are an increasingly used ENM as a component of fluorescent imaging, biosensing, LED screens and solar power cells.[3,4] Consequently, the increasing uses of QDs-enabled products are expected to result in the release of these materials into the environment,[5,6] leading to concern over negative interactions with biota. The cytotoxicity of CdS QDs was reported in prokaryotic and eukaryotic systems and was attributed to oxidative stress.[7-10] Importantly, release of Cd ions from these nanoparticles has been shown to be minimal and as such, the mechanisms of CdS QDs toxicity remains unknown.[11-13] Utilizing the unicellular eukaryote *Saccharomyces cerevisiae*, we demonstrated that one of the pathways for CdS QDs uptake involved the formation of biologically derived "corona" proteins, which actually are not involved in the uptake of ionic Cd (II).[14]

Separately, the model plant *Arabidopsis thaliana* (L.) Heyhn[15] was previously used to investigate CdS QDs phytotoxicity. Accession Landsberg erecta lines, mutagenized with the Maize transposon Ac/Ds,[16] were screened for resistance to CdS QDs in comparison to the wild type: two tolerant mutants (*atnp01* and *atnp02*) were found and characterized genetically and phenotypically.[11] In the work by Marmiroli et al., 2014,[11] two mutant lines were found to

exhibit normal growth, respiration and photosynthesis at 80 mg L^{-1} of CdS QDs which was established as the MIC_{50} value for the wt plants.[11] The main characteristics of the two mutant lines are summarized in the Electronic Supplementary Information (ESI) Tables S1a,b. The two mutant lines were used throughout the experiment to show any differences in uptake, biotransformation, and detoxification in treatments with CdS QDs or $CdSO_4$.

Improving the knowledge of CdS QDs physical state and binding moieties within plant cells will improve the general understanding of how these contaminants interact with organisms, including both metabolically and in terms of mechanisms of toxicity. For example, Cd divalent ions have been known to be toxic for to biota since the early 1970s due to their interference with basic metabolic processes such as respiration and protein.[17] However, CdS QDs have been demonstrated to be highly stable and to exert effects on plant transcription and metabolism in ways that differ markedly from Cd^{2+}.[11,13] Plants have been shown to take up CdS QDs and translocate the particles to aerial tissues, inducing reactive oxygen species (ROS) formation that was detrimental to plant metabolism.[13] Importantly, the fate and speciation of CdS QDs within plant cells is unknown. The CdS QDs could either retain their nano-crystal structure when internalized by cells, or could be disassembled and transformed in less complex structures after processes such as corona protein formation.[14] It is also possible that CdS QDs could be biologically modified or chelated by cell biomolecules through interactions with specific moieties that minimize their toxicity such as anthocyanins, heat shock proteins, and all the molecules produced in response to the oxidative stress caused by the QDs.[13] Such post-uptake structural molecular changes involve specific differences in Cd bonds, including both bond distances and nature of ligands. Important information on these processes can be obtained through Extended X-ray Absorption Fine Structure (EXAFS) analysis.[18,19] This approach can increase understanding of the state of Cd after CdS QDs or $CdSO_4$ accumulation and translocation within *A. thaliana* mutants and wild type lines,

including which moieties are responsible for the interaction between Cd (as QDs or as ions) and molecules. This information can also be used to establish methods for safe removal of QDs from the environment, either with conventional (physico-chemical) methods or with bio/phytoremediation (Cota-Ruiz et al., 2018).[20-22] The main objectives of this study are: a) to clarify whether Cd retains its nanocrystal structure within plant tissues treated with CdS QDs, b) to identify the potential biomolecules chelating the Cd ions released, and c) to investigate if Cd is partially or fully integrated into new nanostructures that differ from the original CdS QDs. The implications for all of these processes, their phytotoxicity, and environmental safety are discussed.

MATERIALS AND METHODS

Plant growth

All reagents were purchased from Sigma-Aldrich (St. Louis, MO, USA) unless otherwise stated. Seedlings of *Arabidopsis thaliana* (L.) Heynh ecotype Landsberg erecta (Ler-0) wild type (wt) and the two mutant lines *atnp01* and *atnp02* were grown on a Murashige and Skoog (MS) nutrient medium (Duchefa Biochemie, Haarlem, NED) containing 1% w/v sucrose and that had been solidified with 0.8% w/v agar at 24°C, 30% relative humidity, and 16h photoperiod (light intensity 120 μM m^{-2} s^{-1} photosynthetic photon flux).[11] In ESI Tables S1a,b are shown physiological and molecular features of the mutants *atnp01* and *atnp02* (Inhibition concentrations, cell viability, photosynthetic activity, relevant genes affected by the transposition). After 10 days of growth on non-treated MS medium, the seedlings were transferred to media amended with a CdS QDs or $CdSO_4$; untreated control plants were maintained in non-amended media. To prevent nanoparticles agglomeration, CdS QDs were sonicated for 30 minutes by ultrasonic bath USC500T (VWR, Radnor, PA, USA). The treatments were established utilizing as reference the minimum growth inhibiting

concentration (MIC) previously determined by Marmiroli et al. (2014):[11] CdS QDs ¾ MIC = 60 mg L^{-1}, $CdSO_4$ ¾ MIC = 150 μM or 115.35 mg L^{-1} $CdSO_4 \cdot 7H_2O$. The effective Cd dose administered to the plants was 46.8 mg L^{-1} for CdS QDs and 16.91 mg L^{-1} for the Cd salt. The concentrations here used were selected because they are sufficient to initiate the response of the wt, as shown in Marmiroli et al., 2020.[23] Plants were harvested after 20 days of treatment. After thorough washing in deionized water, plant fresh weight was measured. The tissues were then oven dried at 80°C until constant weight was reached, and the dry weight was recorded. The plants were then prepared for Cd concentrations measurement as noted below.

Cd concentrations measurement

From 10 petri dish replicates, each containing 25 plants, three replicates of 300 mg (dry weight) aliquot of ground plant material was digested in 10 mL 14.6 M HNO_3 for 20 min at 165°C, followed by 30 minutes at 230°C on a block digester (VELP Scientifica, Usmate, Italy). The resulting solution was subsequently diluted to 6.7 M HNO_3 using distilled water. The plant tissue Cd content was determined by FA-AAS (Flame-Atomic Absorption Spectrometry) (AA240FS) Agilent Technologies, Santa Clara, CA, USA) at 228.8 nm. The recording absorbance for each sample was converted to Cd concentrations via a calibration curve based on a standard solution of high purity (>99%) Cd (Agilent Technologies, TO, Italy). All analyses were performed in triplicate.

X-ray Absorption Spectroscopy

X-ray Absorption Spectroscopy (XAS) measurements at the Cd K-edge (26711.2 eV) were performed at the LISA CRG beamline (BM08)[24] at the European Synchrotron Radiation Facility (ESRF, Grenoble, France) during two experimental sessions using plant samples and several standard model compounds. The main optical features of the beamline were a fixed

exit monochromator with a pair of Si (111)] crystals (energy resolution $\Delta E/E \approx 1.33*10^{-4}$); Pt-coated mirrors were used for harmonics rejection (*E* cutoff ≈ 40 K*e*V). Energy was calibrated with a Cd reference foil (26711.2 eV). Spectra of samples were acquired at room temperature with a constant k step of 0.05 $Å^{-1}$ up to a maximum k value of 15 Å and 18 $Å^{-1}$ for plant tissues and model compounds, respectively. Plant samples were measured in the fluorescence mode with a 12-element HP-Ge detector[25] while model compounds were measured in transmission mode. In all cases, at least two scans were collected for transmission and 8 for fluorescence.

For analysis, tissues of *Arabidopsis thaliana* (acc. Landsberg erecta, Ler-0) wild type (wt) and CdS QDs-tolerant mutant lines (*atnp01* and *atnp02*) in the form of fine dried powder, were pressed in 150 mg pellets. Inorganic model compounds used included CdS QDs, Cd bulk, $CdSO_4$, $CdNO_3$ and $CdCO_3$. The samples were mixed with pure cellulose powder (Sigma Aldrich) and pressed in 1.3 cm diameter pellets using an amount of material sufficient to keep the total absorption (μ) $\leq$1.5 above the edge.

ATHENA software[26] was used to calibrate the energy and to average multiple spectra. Standard procedures were followed to extract the structural extended X-ray absorption fine structure: (EXAFS) signals ($k \bullet \chi(k)$), including pre-edge background removal, spline modelling of bare atomic background, edge step normalization, and energy calibration.[27] Model atomic clusters centered on the absorber atom were obtained by ATOMS;[28] theoretical amplitude and phase functions were generated using the FEFF8 code.[29] EXAFS spectra were fitted through the ARTEMIS software[26] in the Fourier-Transform (FT) space.

Statistics analysis

After checking for normality and homogeneity of variance using Shapiro-Wilks and Levene tests, respectively, data were processed with ANOVA evaluation, followed by Tukey's HSD

post hoc test. In case of non-homogeneity of variance, a Student's t-test was applied. All the calculations were performed with the software IBM SPSS v.24

RESULTS AND DISCUSSION

Nanoparticle characterization

The majority of the CdS QDs ENM (engineered nanomaterials) characterization data is reported in the Electronic Supplementary Information, ESI Figures S1-S4. The EXAFS characterization is reported in Figure 1 and Tables 1, 2 and is discussed below. From the XRD (X-Ray Diffraction) and HR-TEM (High Resolution Transmission Electron Microscope) measurements, the average static diameter was 5 nm, and the crystal structure was that of hexagonal wurtzite (ZnS) with approximately 78% Cd. Average particle size *dh* (hydrodynamic diameter) of the aggregates measured with DLS (Diffraction Light Scattering) and zeta potential (ζ) in ddH_2O (double-deionized water), performed by Zetasizer Nano Series ZS90 (Malvern Instruments, Malvern, UK), were estimated in double-deionized water at 178.7 nm and +15.0 mV, respectively. Overall, since the zeta potential is a Gaussian function, this means that a part of the QDs formed aggregates, the biggest with a diameter of 178.7 nm, but most of the other QDs remained free in small aggregates.

Plant biomass and Cd concentrations in wild type and mutants

Figures 2a,b,c showed the fresh and dry weights as well as the water content of the plants (wt, *atnp01, atnp02*) across the various treatments and for the wt control. The average mass for untreated wt, was 160 mg fresh weight (fw) and 15 mg dry weight (dw), with a water content of 14 g g^{-1}. Plants treated with CdS QDs were all significantly different from the controls for both fresh and dry weight, as well as for their water content, after a treatment of 60 mg L^{-1} for CdS QDs and 115.35 mg L^{-1} for $CdSO_4 \cdot 7H_2O$. The fresh biomass of the CdS QDs-treated

plants was not statistically different among the mutants and the wt, but it was significantly different from the untreated wt. Treatment with $CdSO_4$ did not show any difference in neither fw and dw between wt nor mutants, but they are all significantly different from the wt untreated (Figure 2 a,b). The mutants have the same dw as the untreated wt control when exposed to the QDs treatment, whereas the wt treated with QDs had almost half of the dw of the control untreated (Figure 2 a,b). The difference in water content between wt and mutants reduced the ratio between fresh and dry weight (Figure 2c). In general, the plants grown on CdS QDs had more water content than those grown on $CdSO_4$. Taken together, the data indicate that treatment with CdS QDs caused a slight stress that increased the biomass in the mutants, but not in the wt, while $CdSO_4$ caused modest phytotoxicity in both the wt and mutants (Figure 2 a, b, c). Figure 2d shows the tissue Cd concentrations for each treatment and for the wt control. Both wt and mutants treated with CdS QDs accumulated significantly less Cd than those treated with $CdSO_4$, even though the effective amount of Cd administered was higher as QDs than as that administered as salt. On average the concentrations for the CdS QDs treated plants was between 2-2.1 mg g^{-1}, whereas plants from the $CdSO_4$ treatment had between 2.8 and 3.1 mg g^{-1} (Figure 2d). Among the two different groups treated with CdS QDs or $CdSO_4$, it is likely that there were no differences in the Cd concentrations of wt and mutants because the plants were grown on a semi-inhibiting concentration of each treatment, as opposed to concentrations where more significant toxicity occurred such as shown in ESI Table S1a,b. Results are consistent with the previous work (Marmiroli et al., 2020),[23] which was primarily focused on the morphological and the physiological response to CdS QDs exposure.

X-ray Absorption Spectroscopy

X-ray Absorption Near Edge Structure (XANES) spectra are shown for comparison in Figure 3. EXAFS spectra of the measured samples and associated reference compounds are shown in Figure 1; the main spectral features of the samples do not show any large differences between the wild type and the mutants; the primary differences seem indeed related to the type of Cd exposure. Samples grown on CdS QDs show features fairly consistent with those of CdS QDs particles, although slightly longer periods of EXAFS oscillation are detectable (Figure 1a). This characteristic is even more evident in the spectra of samples grown on $CdSO_4$, which seem to have an oscillation period intermediate between that of CdS QDs and that of $CdSO_4$, where Cd is only bonded to oxygen atoms.[30] The observation of the Fourier transformed spectra (Figure 1b, uncorrected for phase shift) highlights these features; the maxima of FT (Fourier Transformed) first shell peaks of the studied samples lie at intermediate R values between those of $CdSO_4$ and CdS. Importantly, none of the plant samples shows signs of a higher coordination shell. The spectra of all plant samples were then fitted to a mixed O/S first shell starting from two models obtained using the crystallographic structure reported by Sowa (2005)[31] and Wyckoff (1963)[32] for CdS and CdO, respectively. Note that in principle, EXAFS cannot discriminate among atoms with similar Z such as N, O and F or P, S and Cl. In such a system however, the presence of chloride or phosphide can be safely excluded since they would be present in an oxidized form; F can be also excluded given its low abundance in the system. The occurrence of N as a direct Cd ligand, which cannot be excluded nor from redox considerations, nor from chemical abundance, can be safely excluded on the basis of crystal-chemical considerations based on the bond valence theory (see discussion below). Fits were performed fixing the many-body amplitude reduction factor (S_0^2) to the value obtained with the fit of CdS QDs, leaving the path degeneracy free to vary. In order to facilitate comparison among all the samples, the same *k* range (3.0-12.0 $Å^{-1}$) was used for all fits. The multiparameter fit results are reported in Table 1. As an example, Figure 4 shows the Cd *K*-

edge EXAFS and Fourier transform data together with the corresponding multiparameter fits of the mutant *atnp01* and of the model compounds CdS QDs and $CdSO_4$.

Cd coordination in *A. thaliana*

The EXAFS quantitative analysis reveals a complex average environment for Cd in the samples, with Cd bonded to both S and O atoms in plants grown on CdS QDs and $CdSO_4$. Based on the analysis performed, no distinction can be made between the *A. thaliana* wild type and the mutant lines. On the other hand, Cd coordination differs substantially depending on the type of Cd exposure; this is clearly evident by looking at both the Cd-O and Cd-S bond distances and at the S/O ratio for the first coordination shell (Table 1). Specifically, while Cd-S distance does not vary substantially, Cd-O distance shows considerable difference, ranging from ≈2.16 Å in samples grown on CdS QDs to ≈2.22 Å in those grown on $CdSO_4$. Moreover, the number of Cd-O and Cd-S bonds in plants grown on CdS QDs strongly favors Cd-S (≈90% Cd-S and 10%Cd-O), whereas for plants grown on $CdSO_4$ this ratio is closer to 1:1.

However, coordination numbers obtained from EXAFS have lower accuracy because of correlation with other parameters affecting the amplitude of the EXAFS oscillation, specifically the many-body amplitude reduction factor (S_0^2), which was fixed for this reason, and the Debye-Waller factor (σ^2). Results can be thus confounding, and as such, approximately 20% of accuracy is typically assumed for coordination numbers. Moreover, the contribution of light oxygen backscatterer is difficult to analyze because of the dominant backscattering from S atoms.

Considerations based on crystal-chemical comparisons and on the bond-valence (B.V.) method can be used to strengthen fit results.[33,34] The B.V. approach relies on the fact that in general, the bond length is a function of bond valence, thus providing a tool for the interpretation of bond lengths (*cf.* Table 1, 2). According to this model, the valence (v_{ij}) of a

bond between two atoms *i* and *j* is defined so that the sum of all the valences from an atom *i* with valence $\mathbf{V}_i$ obeys the equation:

$$\Sigma_j v_{ij} = \mathbf{V}_i. \quad (1)$$

The most commonly employed empirical expression for the variation of the length d_{ij} of a bond with valence is:

$$v_{ij} = \exp[(\mathbf{R}_{ij} - d_{ij})/\mathbf{b}] \quad (2)$$

where **b** is commonly considered a constant equal to 0.37 Å and $\mathbf{R}_{ij}$ is the bond-valence parameter.[28] Knowing the valence of Cd (nominally Cd^{2+}), the bond distances Cd-O and Cd-S and the bond valence parameters ($\mathbf{R}_{CdS}$ and $\mathbf{R}_{CdO}$), it is then possible to estimate the number of bonds required to satisfy Cd valence. It must be emphasized that bond valence parameters are strictly empirical and several parameters can be found in the literature for most elements. In this study, we used the bond valence parameters reported by Palenik (2006)[35] since they lead to the closest accord between theoretical and experimental values in model compound CdS and $CdSO_4$.

Table 2 shows the bond-valence values for Cd-S and Cd-O bonds for Cd atoms in each sample. The relative bond valence sums (Σ B.V.) for Cd were calculated employing the number of Cd-O and Cd-S bonds obtained by the EXAFS analysis. Bond valence sums (BVS) are fairly close to the 2 v.u. (valence unit) necessary to neutralize Cd (II) charge, especially considering the ~0.1 v.u. discrepancy shown by CdS model compound. Note that the bond valence parameter for Cd-N bonds (1.96 Å)[34] is significantly higher than that for Cd-O (ranging from 1.875 to 1.904 Å)[34,35] and would then lead to BVS much higher than 2, thus strongly pointing towards the presence of only O as the main ligand, together with S.

Indeed, the total coordination number (O+S) around Cd atoms required to neutralize Cd charge, estimated by the B.V. method, is in general agreement with that obtained by EXAFS. These results can be compared with known Cd compounds in order to hypothesize a

prevailing coordination environment. Several organic and inorganic compounds with CdS_xO_y coordination are reported in the literature.[36-38] The growth of plants on $CdSO_4$ seems to be compatible with many mixed Cd-S/O polyhedra reported in the literature (Table 3). Specifically, distances very close to those observed in specimens from this study are reported for compounds described by Zhang et al. (2012)[39] and Xu et al. (2015)[40] in CdS_3O polyhedra and by Zhang et al. (1999, 2000)[41,42] and Beheshti et al. (2007)[43] in CdS_2O_2 polyhedra. Conversely, plants grown on CdS QDs show, an unusual combination of rather short distances, both for Cd-S and Cd-O bonds. To the best of our knowledge, such bond lengths have only been reported by Phillips et al. (1995)[44] in the CdS_2O_2 polyhedra of a Cd diisopropyl monothiophosphate (Table 3).

Molecular environment of Cd

EXAFS data indicate that the pristine structure of CdS QDs was not preserved in the plants and, after uptake, the particles are biotransformed (Figures 1, 3), although some of the molecular complexity is retained. Cd-S bond distances are indeed significantly shorter with respect to the Cd-S bond in the CdS QDs structure (≈2.48 vs. ≈2.52 Å); moreover, it is possible to notice the formation of additional Cd-O bonds. The biotransformation occurs for both $CdSO_4$ and for the CdS QDs that are inside the plant and involves different mechanisms based on the different substrates: in the former case Cd (II) ions were released and bonded by either S or O as nearest neighbors in similar proportions, while in the latter, a more complex biotransformation should have occurred to the nanostructure containing the Cd atoms, because of the biochemical complexity of the plant cell.

Interestingly, the mutants and wt showed the same Cd coordination, suggesting that the resistance to CdS QDs in *atnp01* and *atnp02* does not depend on a different ability to biotransform CdS QDs but on detoxification and on selective storage.

It seems that this biotransformation was a late event after the manifestation of tolerance and did not differ in wt and mutants.

Cadmium shows a high affinity for thiol-containing compounds, including glutathione, phytochelatins and sulfur-containing amino acids;[45-47] however Cd-S bonds in those molecules are generally longer than those observed herein. Other EXAFS studies on Cd uptake in plants also show a unique local Cd environment. Several studies have focused in *Salsola kali* (tumbleweed),[48-50] which has a high capacity to take up and translocate Cd to the aerial parts and also possess a uniquely high content of thiols. De la Rosa et al.[48] reported for this plant, in an EXAFS study, Cd-O/Cd-S distances comparable to those observed in the present study (Table 4) and suggested their findings were indicative of small organic acid association that facilitated Cd translocation from roots to stems and leaves and that separate Cd-phytochelatin complexes may also form. The distances observed in stems of *S. kali* resemble those of *A. thaliana* grown on $CdSO_4$, whereas the Cd environment in *S. kali* leaves resembles samples grown on CdS QDs. *Zygophyllum fabago* L. (Syrian beancaper) is a succulent, perennial shrub found in metal-contaminated soils and disturbed sites; it is a known Cd hyperaccumulator and is also Cd tolerant.[51-53] The Cd atomic environment according to EXAFS analyses of both roots and shoots indicates bond lengths that are quite close to those of *A. thaliana* grown on CdS QDs (Table 4). The authors hypothesized that for *Z. fabago*, the response to Cd exposure involved concentrating Cd ions in less metabolically active tissues through binding to non-protein thiol compounds.[52-53]

It has been reported that the proportion of Cd coordinated by sulfur atoms is poor in hyperaccumulators,[38,45,47,54,55] and that the majority of Cd is bonded by oxygen atoms provided by other molecules present in the cell.[38] In *A. thaliana* grown on CdS QDs, a remarkably unique response was observed, characterized by the significant prevalence of Cd-S bonds similar to what observed in *Z. fabago* roots.[53]

The speciation of metals such as Zn and Cd in plants has been reported a number of times, often with salt/ionic exposure and with XAS and micro-fluorescence.[53,56] Only a limited number of studies have used EXAFS analyses on plants exposed to engineered nanomaterials.[57,58] The present study finds that the behavior of Cd when in the QDs form is completely different than when it is in the salt form, which is consistent with prior results observed in both model plants and crop species,[11,59,60,61] where ion release from QDs to the solution/growth medium was minimal. Although significant differences were observed between hyperaccumulators and non-hyperaccumulators,[38,56] there was a consistent prevalence of Cd-O bonds over Cd-S bonds. The present study with CdS QDs shows no differences between wt and the tolerant mutants on this point. Considering that uptake and were also sequentially separated in this system, these findings along with our previous '-omics' level work[11,59] provide further evidence that internal biotransformation of CdS QDs occurred through an alternative pathway (Figure 5)

Role of oxygen- and sulfur-containing molecules in Cd bonding within the cell

Plant sulfur metabolism is known to be a particularly complex set of processes. Once sulfate (SO_4^{2-}) is taken up from the soil solution by specific root membrane transporters (SULTR1-5), it is either temporarily accumulated in the cell vacuoles of roots and shoots, or it enters the sulfate reductive metabolic pathway.[62] Between the initial stages of sulfate uptake into root cells and its reduction in leaf chloroplasts that constitute the principal sites of assimilation,

significant cell-to-cell transport through plasmodesmata and numerous transmembrane inter- and intracellular transporters occurs with the utilization of different classes of enzymes.[62]The coordination of short and long-distance sulfur transport requires specific signaling mechanisms to control and regulate all the genes encoding proteins involved in the assimilation pathways.[63] As a mechanism of the QDs biotransformation, the particle's S atoms may associate with free molecules such as proteins or secondary metabolites. This type of transformation may recruit the particles into sulfur homeostasis processes that cause a break-down of the QDs crystal structure and release some Cd (II) ions along with a large number of CdS_n clusters that are either in the form of amorphous nanostructures or bound with small oxygen-containing molecules present in the cell.[38,56]

Cd complexes with molecules bearing thiol groups show similar mixed bonding;[36,37,45,46] while Cd-S distances are only slightly higher than those reported in this study, Cd-O distances are significantly lower. Considering that a cell contains a huge number of small and large molecules associated with secondary metabolism,[64] the amount of O ligands (or both S and O) such as glucosinolates and sulfulipids that are available for bonding Cd ions at these distances would likely be variable depending on the structure of the molecule.[65-67] In addition, structures such as cellulose, pectin and the cell wall, during its formation, are somewhat flexible and may form very different Cd-O/-S bonds depending on local conditions; a similar situation was observed with Pb atoms in walnut roots.[68] The case of *A. thaliana* grown on CdS QDs indicates a preference for Cd-S bonds, thus suggesting significant Cd association with thiol groups. According to the considerations highlighted in the paragraph discussing Cd coordination, the shorter Cd-O bonds observed may simply be the effect of the presence of oxygen-coordinated Cd sites with a lower coordination of a smaller fraction of O ligands as compared to those reported in the literature. Indeed, in the presence of a smaller amount of anionic ligands, the valence of Cd-O bonds, in order to

balance Cd positive charge, have to increase by reducing the bond distance, thus resulting in a shorter Cd-O bond.

It is possible to hypothesize several mechanisms for CdS QDs interaction with plant cell structures during uptake and cellular response (sensitivity/tolerance), biotransformation, and detoxification as depicted in Figure 5. These steps may be consequential in time, but they are genetically independent. CdS QDs enter the cell at the early "exposure" phase and some particles are packaged into vesicles or associated with different types of molecules, including corona proteins, secondary metabolites and enzymes such as HSP proteins. The cellular response to CdS QDs uptake generates a large amount of ROS that may subsequently impact mitochondria, chloroplasts and membrane functionality if it is not triggered an anti-oxidative stress tolerance response, as that based on the genetic function identified with the mutants *atnp01* and *atnp02* (Marmiroli et al., 2014).[11] At the molecular level, it has been demonstrated that this response is driven by the activation of genes and proteins involved in ROS detoxification and in general defense response.[11,59,69,70] These early events and the adjustment of cellular functions that follow a new transcriptional modulation,[11] are followed by a late phase in which QDs are reduced in complexity and toxicity, which can be defined a biotransformation phase, with the liberation of bio-modified CdS QDs structures and a reduced amount of Cd (II) ions. As part of a further "detoxification" process, the Cd atoms that remained attached to the bio-modified nanostructures form stabilizing bonds with S and O atoms present within defense molecules produced as a consequence of the increased ROS production. It is complicated to state whether Cd-S or Cd-O bonds are more stable because this is a complex biological system with the presence of multiple molecules (organic acids, enzymes, small and large secondary metabolites, and lipids) that can affect the bond stability. In addition, it is important to bear in mind that, since the EXAFS signal represents the average of potentially different Cd environments, it is not possible to ascertain whether bio-

modified CdS clusters form only one type of molecule with mixed O/S bonding or our results reflect the average of different bonding environments with variable proportions of ligand molecules that can contain O or S bonding atoms.

CONCLUSIONS: Environmental implications

The current study used EXAFS to demonstrate that there is a range of molecules that bind to and detoxify CdS QDs and Cd ions, largely by chelating the quantum dots and ions through their O and S atoms.

Importantly, the combination of physical, physiological, and molecular methods allowed some conclusions to be drawn on the intracellular fate of CdS QDs. Genetic (mutants tolerant to CdS QDs) and spectroscopic (EXAFS spectroscopy) measurements were used to identify relationships between uptake, tolerance and changes in the structure of CdS QDs, as well as the atomic binding and subsequent biotransformation (Figure 5).[11,23,59,61,69,70]

From an environmental perspective, information on CdS QDs biotransformation is particularly important. There is significant evidence that CdS QDs release very low amount of Cd ions, and as such, differ markedly from the corresponding $CdSO_4$ as measured by a range of endpoints. The current study provides rationale at the atomic and molecular scale for that behavior.

The increasing amount of CdS QDs produced for a range of markets raises concern over environmental release and contamination dispersion,[5,6] and has begun to stimulate research into decontamination strategies, including bioremediation and phytoremediation.[20-22]

A thorough analysis of the fate of QDs within plant systems shows that Cd within the QDs remains largely bound to different organic molecules rather than being released in free ions. This discovery increases the potential for using biological remediation strategies. A different

fate exists for the Cd atoms released from CdSO4,[11,23,59] since in this case, due to the high solubility of $CdSO_4$, Cd is directly taken up as ionic Cd. Cd^{2+} free ions are more easily available for bonding with other molecules in the plant cells and, hence, their toxicity is greater, suggesting that alternative remediation strategies need to be used in such contamination scenario.

Importantly, the interactions between *A. thaliana* and QDs must now be investigated in other plant species (i.e., crop and tree species) that are relevant from an economic and environmental perspective. Particular care should be taken to evaluate the impact of these unique *in planta* processes on the fate of QDs and other ENMs in the environment, taking into account both issues of food chain contamination and the potential for effective remedial strategies, as phytoremediation.[65,71-74]

ELECTRONIC SUPPLEMENTARY INFORMATION

Electronic Supporting information (ESI) includes methods related to the "CdS QDs synthesis and characterization". Figure S1: HR-TEM and XRD images. Figure S2: HR-TEM images. Figure S3: ESEM and EDX images. Figure S4: CdS QDs size dispersion. Table S1: characteristics of the *A. thaliana* mutants *atnp01* and *atnp02*.

ACKNOWLEDGEMENTS

The authors acknowledge the Italian CRG beam-line at ESRF (LISA-BM08) and its staff for provision of the beam-time and assistance during the experiment (08-01 1041). The authors wish to thank G. Lencioni of the University of Parma for helping growing *A. thaliana* plants

and A. Zappettini from IMEM-CNR for helping with the CdS QDs synthesis. JCW acknowledges USDA NIFA Hatch CONH00147.

The authors declare no competing financial interest.

References

1. Caballero-Guzman, A.; Nowack, B. A critical review of engineered nanomaterial release data: Are current data useful for material flow modeling? *Environ Pollut* 2016, **213**, 502-517.
2. Inshakova, E.; Inshakov, O. World market for nanomaterials: Structure and trends. *MATEC Web Confer*. 2017, **129**, 02013, doi:10.1051/matecconf/201712902013.
3. Aroutiounian, V.; Petrosyan, S.; Khachatryan, A.; Touryan, K. Quantum dot solar cells. *J Appl Phys* 2001, **89**, 2268-2271
4. Bu, Y.; Chen, Z.; Li, W.; Yu, J. High-efficiency photoelectrochemical properties by a highly crystalline CdS-sensitized ZnO nanorod array. *ACS Appl Mater Inter* 2013, **5**, 5097-5104
5. Gensch, C. O.; Baron, Y; Blepp, M. 2016. Study to assess 2 RoHS exemption requests [#1 Cadmium in colour converting II-VI LEDs (<10 μg Cd per mm2 of light-emitting area) for use in solid state illumination or display systems (Request

for renewal of Exemption 39 of Annex IV of Directive 2011/65/EU); #2 Cadmium in LCD Quantum Dot Light Control Films and Components].

6. Vance, M.E.; Kuiken, T.; Vejerano, E. P.; McGinnis, S. P.; Hochella, M. F.; Rejeski, D.; Hull, M. S. Nanotechnology in the real world: Redeveloping the nanomaterial consumer products inventory. *Beilstein J. Nanotechnol* 2015, **6**, 1769–1780.
7. Chen, N.; He, Y.; Su, Y.; Li, X; Huang, Q.; Wang, H.; Zhang, X.; Tai, R.; Fan, C. The cytotoxicity of cadmium-based quantum dots. *Biomaterials* 2012, **33**, (5), 1238-1244.
8. Reddy, P. V. L.; Hernandez-Viezcas, J. A.; Peralta-Videa, J. R.; Gardea-Torresdey, J. L. Lessons learned: Are engineered nanomaterials toxic to terrestrial plants? *Sci Tot Environ* 2016, **568**, 470–479.
9. Pagano, L.; Caldara, M.; Villani, M.; Zappettini, A.; Marmiroli, N.; Marmiroli, M. In Vivo-In Vitro Comparative Toxicology of Cadmium Sulphide Quantum Dots in the Model Organism *Saccharomyces cerevisiae*. *Nanomaterials* 2019, **9**, 512-529.
10. Paesano, L.; Perotti, A.; Buschini, A.; Carubbi, C.; Marmiroli,M.; Maestri, E.; Iannotta, S.; Marmiroli, N. Markers for toxicity to HepG2 exposed to cadmium sulphide quantum dots; damage tomitochondria. *Toxicology* 2016, **374**, 18−28.
11. Marmiroli, M.; Pagano, L.; Savo Sardaro, M. L.; Villani, M.; Marmiroli, N. Genome-wide approach in *Arabidopsis thaliana* to assess the toxicity of cadmium sulfide quantum dots. *Environmental Sci Techno* 2014, **48**, (10), 5902-5909.
12. Marmiroli, M.; Pagano, L.; Pasquali, F.; Zappettini, A.; Tosato, V.; Bruschi, C. V.; Marmiroli, N. A genome-wide nanotoxicology screen of *Saccharomyces cerevisiae* mutants reveals the basis for cadmium sulphide quantum dot tolerance and sensitivity. *Nanotoxicology*, 2016, **10** (1), 84-93.

13. Pagano, L.; Maestri, E.; White, J. C.; Marmiroli, N.; Marmiroli, M. Quantum dots exposure in plants: Minimizing the adverse response. *Current Op Environ Sci Health* 2018, **6**, 71-76.

14. Ruotolo, R.; Pira, G.; Villani, M.; Zappettini, A.; N. Marmiroli. Ring-shaped corona proteins influence the toxicity of engineered nanoparticles to yeast. *Environ Sci Nano*, 2018, **5**, 1428-1440.

15. Takou, M.; Wieters, B.; Kopriva, S.; Coupland, G.; Linstädter, A.; de Meaux, J. Linking genes with ecological strategies in *Arabidopsis thaliana*. *J Exp Bot* 2019, **70**, (4), 1141–1151.

16. Long, D.; Martin M.; Sundberg E.; Swinburne J.; Puangsomlee P.; Coupland G.. The maize transposable element system Ac/Ds as a mutagen in Arabidopsis: Identification of an albino mutation induced by Ds insertion. Proc. Natl. Acad. Sci. USA. 1993, **90**, 10370-10374

17. Flick, D. F.; Kraybill, H. F.; and Dlmitroff, J. M. Toxic effects of cadmium: a review. *Environ* Res 1971, ***4***, (2), 71-85.

18. Sarret, G.; Pilon Smits, E. A. H.; Castillo Michel, H.; Isaure, M. P.; Zhao, F. J.; Tappero, R. Chapter One - Use of Synchrotron-Based Techniques to Elucidate Metal Uptake and Metabolism in Plants. *Adv Agron* 2013, **119**, 1-82.

19. Avellan, A.; Simonin, M.; McGivney, E.; Bossa, N.; Spielman-Sun; E., Rocca, J. D.; Bernhardt, E.S.; Geitner, N. K.; Unrine, J. M.; Wiesner, M.R.; Lowry, G. V. Gold nanoparticle biodissolution by a freshwater macrophyte and its associated microbiome. *Nat nanotech* 2018, **13**, 1072–1077.

20. Yeo K.-M.; Nam D.-H. Influence of different types of nanomaterials on their bioaccumulation in a paddy microcosm: A comparison of TiO2 nanoparticles and nanotubes. Environ pollut 2013. **178**, 166-172.

21. Cota-Ruiz K.; Delgado-Rios C.; Martinez-Martinez A.; Núñez-Gastelum J.A.; Peralta-Videa J.R.; Gardea-Torresdey J.L. Current findings on terrestrial plants – Engineered nanomaterial interactions: Are plants capable of phytoremediating nanomaterials from soil? C.O.E.S.H. 2018. **6**, 9-15.

22. Huang Z.; Zeng Z.; Chen A.; Zeng G.; Xiao R.; Xu P.; He K.; Song Z.; Hu L.; Peng M.; Huang T.; Chen G. Differential behaviors of silver nanoparticles and silver ions toward cysteine: Bioremediation and toxicity to Phanerochaete chrysosporium. Chemosphere 2018. **203**, 199-208.

23. Marmiroli, M.; Mussi, F; Pagano, L; Imperiale, D.; Lencioni, G.; Villani, M; Zappettini, A.; White, J. C.; Marmiroli, N. Cadmium sulfide quantum dots impact *Arabidopsis thaliana* physiology and morphology. Chemosphere 2020, **240**, 124856.

24. d'Acapito, F., Lepore, G.O., Puri, A., Laloni, A., La Mannna, F., Dettona, E., De Luisa, A., Martin, A. The LISA beamline at ESRF. *J. Synchrotron Radiat.* 2019, **26**, 551-558.

25. Puri, A.; Lepore, G. O.; d'Acapito, F. The New Beamline LISA at ESRF: Performances and Perspectives for Earth and Environmental Sciences. *Condens Matter* 2019, **4**, 12-19.

26. Ravel, B.; Newville, M., A.T.H.E.N.A. ATHENA, ARTEMIS, HEPHAESTUS: data analysis for X-ray absorption spectroscopy using IFEFFIT. J Synchr Rad 2005, **12**, 537-541.

27. Lee, P. A.; Citrin, P. H.; Eisenberger, P. T.; Kincaid, B. M. Extended x-ray absorption fine structure - its strengths and limitations as a structural tool. *Revi Mod Phys* 1981, **53**, 769-806.

28. Ravel, B. ATOMS: crystallography for the X-ray absorption spectroscopist. J Synchr Rad 2001 **8**, 314–316.
29. Ankudinov, A.L.; Ravel, B.; Rehr, J.J.; Conradson, S.D. Real-space multiple-scattering calculation and interpretation of x-ray-absorption near-edge structure. *Phys Rev B* 1998, **58**, 7565-7576.
30. Kokkoros, P. A.; Rentzeperis, P. J. The crystal structure of the anhydrous cadmium and mercuric sulfates. *Z Kristallogr Cryst Mater* 1964*,* **119**, (1-6), 234-244.
31. Sowa, H. On the mechanism of the pressure-induced wurtzite-to NaCl-type phase transition in CdS: an X-ray diffraction study. *Solid State Sc* 2005, **7**, 73-78.
32. Wyckoff, R. W. G. Crystal Structures, second edition **1963**. Interscience Publishers, New York, New York.
33. Brown, I. D.; Altermatt, D. Bond-valence parameters obtained from a systematic analysis of the inorganic crystal structure database. *Acta Crystallogr B*, 1985, **41**(4), 244-247.
34. Brese, N.E.; O'Keeffe, M. Bond-valence parameters for solids. *Acta Crystallogr B* 1991, **47**, 192-197.
35. Palenik, G. J. A critical evaluation of homo-and hetero-leptic cadmium complexes using bond valence sums. *Can J Chem* 2006, **84**, 99-104.
36. Jalilehvand, F.; Mah, V.; Leung, B. O.; Mink, J.; Bernard, G. M.; Hajba, L. Cadmium (II) cysteine complexes in the solid state: a multispectroscopic study. *Inorg Chem* 2009, **48**, (9), 4219-4230.
37. Jalilehvand, F.; Leung, B. O.; Mah, V. Cadmium (II) complex formation with cysteine and penicillamine. *Inorg Chem* 2009*, **48**,* (13), 5758-5771.

38. Huguet, S.; Bert, V.; Laboudigue, A.; Barthès, V.; Isaure, M.-P.; Llorens. I.; Schath, H.; Sarret, G. Cd speciation and localization in the hyperaccumulator *Arabidopsis halleri. Environ Exper Bot* 2012, **82**, 54– 65

39. Zhang, Q.; Zheng, S. T.; Bu, X.; Feng, P. Two-Step Synthesis of a Novel Cd_{17} Sulfide Cluster through Ionic Clusters. *Z Anorg Allg Chem* 2012, **638**, (15), 2470-2472.

40. Xu, C.; Hedin, N.; Shi, H. T.; Xin, Z..; Zhang, Q. F. Stepwise assembly of a semiconducting coordination polymer $[Cd_8S(SPh)_{14}(DMF)(bpy)]_n$ and its photodegradation of organic dyes. *Dalton Trans*, 2015, **44**, (14), 6400-6405.

41. Zhang, Y.; Jianmin, L.; Nishiura, M.; Deng, W.; Imamoto, T. Metallohelice: Effects of hydrogen bond interactions on helical morphology. *Che Lett* 1999, **28**, (12), 1287-1288.

42. Zhang, Y.; Li, J.; Chen, J.; Su, Q.; Deng, W.; Nishiura, M.; Imamoto, T.; Wu, X.; Wang, Q. A novel α-helix-liked metallohelicate series and their structural adjustments for the isomorphous substitution. *Inorg Chem* 2000, **39**, (11), 2330-2336.

43. Beheshti, A.; Clegg, W.; Dale, S. H.; Hyvadi, R. Synthesis, crystal structures, and spectroscopic characterization of the neutral monomeric tetrahedral $[M(Diap)_2(OAc)_2]\cdot H2O$ complexes (M= Zn, Cd; Diap= 1,3-diazepane-2-thione; OAc= acetate) with N–H··· O and O–H··· O intra- and intermolecular hydrogen bonding interactions. *Inorg Chim acta*, 2007, **360**(9), 2967-2972.

44. Phillips, J. R.; Poat, J. C.; Slawin, A. M.; Williams, D. J.; Wood, P. T.; Woollins, J. D. Polymeric and bimetallic complexes of diisopropyl monothiophosphate. *J Chem Soc Dalton Trans* 1995,**14**, 2369-2375.

45. Cobbett, C.; Goldsbrough, P. Phytochelatins and Metallothioneines: Roles in Heavy Metal Detoxification and Homeostasis. *Annu Rev Plant Biol* 2002, **53**, 159–82.

46. Gallego, S. M.; Pena, L. B.; Barcia, R. A.; Azpilicueta, C. E.; Iannone, M. F.; Rosales, E. P.; Zawoznik, M. S.; Groppa, M. D.; Benavides, M. P. Unravelling cadmium toxicity and tolerance in plants: Insight into regulatory mechanisms. *Environ Exp Bot* 2012, **83**, 33– 46.

47. Park, J.; Song, W.-Y.; Ko, D.; Eom Y.; Hansen, T. H.; Schiller, M.; Lee, T. G.; Martinoia, E.; Lee Y. The phytochelatin transporters AtABCC1 and AtABCC2 mediate tolerance to cadmium and mercury. *Plant J* 2012, **69**, 278–288

48. De la Rosa, G.; Peralta-Videa, J. R.; Montes, M.; Parsons, J.G.; Cano-Aguilera, I.; Gardea-Torresdey, J. L. Cadmium uptake and translocation in tumbleweed (*Salsola kali*), a potential Cd hyperaccumulator desert plant species: ICP/OES and XAS studies. *Chemosphere* 2004, **55**, 1159–1168.

49. Akhani, H., Edwards; G., Roalson, E. H. Diversification of the Old World Salsoleae s.l. (Chenopodiaceae): Molecular Phylogenetic Analysis of Nuclear and Chloroplast Data Sets and a Revised Classification. *Int J Plant Sci* 2007, **168**, (6), 931–956.

50. De la Rosa, G.; Martínez-Martínez, A.; Pelayo, H.; Peralta-Videa, J. R.; Sanchez-Salcido, B.; Jorge L. Gardea-Torresdey, J. L. Production of low-molecular weight thiols as a response to cadmium uptake by tumbleweed (*Salsola kali*). *Plant Physiol Biochem* 2005, **43**, 491–498

51. Lefèvre I.; Corréal E.; Lutts S. Cadmium tolerance and accumulation in the noxious weed Zygophyllum fabago *Can J Bot* 2005, **83**, 1655-1662.

52. Lefèvre, I.; Vogel-Mikuš, K.; Jeromel, L.; Vavpetic, P.; Planchon, S.; Arcon, I.; Van Elteren, J.T.; Lepoint, G.; Gobert, S.; Renaut, J.; Pelicon, P.; Lutts S. Differential cadmium and zinc distribution in relation to their physiological impact in the leaves of the accumulating *Zygophyllum fabago* L. *Plant Cell Environ* 2014, **37**, 1299–1320.

53. Lefèvre, I.; Vogel-Mikuš, K.; Arcon, I.; Lutts, S. How do roots of the metal-resistant perennial bush *Zygophyllum fabago* cope with cadmium and zinc toxicities? *Plant Soil* 2016, **404**, 193–207.

54. Kupper, H.; Mijovilovich, A.; Meyer-Klaucke, W.; Kroneck, P.M.H. Tissue- and Age-Dependent Differences in the Complexation of Cadmium and Zinc in the Cadmium/Zinc Hyperaccumulator *Thlaspi caerulescens* (Ganges Ecotype) Revealed by X-Ray Absorption Spectroscopy. *Plant Physiol* 2004, **134**, (2), 748-757.

55. Vogel-Mikuš, K.; Arcon, I.; Kodre, A. Complexation of cadmium in seeds and vegetative tissues of the cadmium hyperaccumulator *Thlaspi praecox* as studied by X-ray absorption spectroscopy. *Plant Soil* 2010, **331**, 439–451

56. Isaure, M.-P.; Huguet, S.; Meyer, C.-L.; Castillo-Michel, H.; Testemale, D.; Vantelon, D.; Saumitou-Laprade, P.; Verbruggen, N.; Sarret, G. Evidence of various mechanisms of Cd sequestration in the hyperaccumulator *Arabidopsis halleri*, the non-accumulator *Arabidopsis lyrata*, and their progenies by combined synchrotron-based techniques. *J Exper Bot* 2015, **66**, (11), 3201–3214.

57. Servin, A. D.; Castillo-Michel, H.; Hernandez-Viezcas, J. A.; Corral Diaz, B.; Peralta-Videa, J. R.; Gardea-Torresdey, J. L. Synchrotron micro-XRF and micro-XANES confirmation of the uptake and translocation of TiO_2 nanoparticles in cucumber (Cucumis sativus) plants. *Environ. Sci. Technol*. 2012, **46**, 7637−7643.

58. Hernandez-Viezcas, J. A.; Castillo-Michel, H.; Andrews, J. C.; Cotte, M.; Rico, C.; Peralta-Videa, J. R.; Ge, Y.; Priester, J. H.; Holden, P. A.; Gardea-Torresdey, J. L. In situ synchrotron X-ray fluorescence mapping and speciation of CeO2 and ZnO nanoparticles in soil cultivated soybean (Glycine max). *ACS Nano* 2013, **7** (2), 1415−1423.

59. Marmiroli, M.; Imperiale, D.; Pagano, L.; Villani, M.; Zappettini, A.; Marmiroli, N. The Proteomic Response of Arabidopsis thaliana to Cadmium Sulfide Quantum Dorrelation with the transcriptomic response. *Front. Plant Sci*. 2015, **6**, 1104.

60. Pagano, L.; Pasquali, F.; Majumdar, S.; De La Torre-Roche, R.; Zuverza-Mena, N.; Villani, M.; Zappettini, A.; Marra, R. E.; Isch, S. M.; Marmiroli, M.; Maestri, E.; Dhankher, O. P.; White, J. C.; Marmiroli, N. Exposure of Cucurbita pepo to binary combinations of engineered nanomaterials: Physiological and molecular response. *Environ. Sci.: Nano* 2017, **4**, 1579−1590.

61. Majumdar S.; Ma C.; Villani M.; Zuverza-Mena N.;Pagano L.; Huang Y.; Zappettini A.; Keller A. A.; Marmiroli N.; Parkash Dhankher O.; White J.C. Surface coating determines the response of soybean plants to Cadmium Sulphyde Quantum Dots. Nanoimpact 2019. **14**, 100151

62. Takahashi, H.; Kopriva, S.; Giordano, M.; Saito, K.; Hell, R. Sulfur Assimilation in Photosynthetic Organisms: Molecular Functions and Regulations of Transporters and Assimilatory Enzymes *Annu Rev Plant Biol* 2011, **62**, 157–84.

63. Koprivova, A.; Kopriva, S. Sulfation pathways in plants. *Chem-Biol Interact* 2016, **259**, 23-30.

64. Teles Y.C.F.; Sallett M.; Souza R.; Vanderlei de Souza MdF. Sulphated Flavonoids: Biosynthesis, Structures, and Biological Activities. *Molecules* 2018, **23**, 480.

65. Halkier, B. A.; Gershenzon, J. Biology and Biochemistry of Glucosinolates. *Annu. Rev. Plant Biol.* 2006, **57**, 303–33.

66. Radojcic-Redovnikovic, I.; Gliveti, T.; Delonga, K.; Vorkapic-Furac, J. Glucosinolates and their potential role in plant. *Period Biol* 2008, **110**, (4), 297–309.

67. Shimojima, M. Biosynthesis and functions of the plant sulfolipid. *Prog Lipid Res* 2011, **50**, 234–239.

68. Marmiroli, M.; Maestri, E.; Antonioli G., Marmiroli, N. Evidence of the involvement of plant ligno -cellulosic structure in the sequestration of Pb: an X-ray spectroscopy-based analysis. *Environ Pollut* 2005, **134**, 217–227.

69. Pagano, L.; Maestri, E.; Caldara, M.; White, J.C.; Marmiroli, N.; Marmiroli, M. Engineered nanomaterial activity at the organelle level: Impacts on the chloroplasts and mitochondria. *ACS Sustain. Chem. Eng*. 2018, **6**, 12562–12579.

70. Ruotolo, R.; Maestri, E.; Pagano, L.; Marmiroli, M.; White, J. C.; Marmiroli, N. Plant response to metal-containing engineered nanomaterials: an omics-based perspective. *Environ. Sci. Technol*. 2018, **52** (5), 2451−2467.

71. Gardea-Torresdey, J. L.; Rico, C. M.; White, J. C. Trophictransfer, transformation, and impact of engineered nanomaterials interrestrial environments.Environ. Sci. Technol. 2014, **48**(5), 2526−2540.

72. Hawthorne, J.; De la Torre Roche, R.; Xing, B.; Newman, L. A.;Ma, X.; Majumdar, S.; Gardea-Torresdey, J.; White, J. C. Particle-sizedependent accumulation and trophic transfer of cerium oxide througha terrestrial food chain.Environ. Sci. Technol. 2014, **48**, 13102−13109.

73. De la Torre Roche, R.; Servin, A. D.; Hawthorne, J.; Xing, B.; Newman, L. A.; Ma, X.; Chen, G.; White, J. C. Terrestrial trophictransfer of bulk and nanoparticle

La2O3 does not depend on particlesize.Environ. Sci. Technol. 2015, **49**(19), 11866−11874.

74. Servin, A.D.; Pagano, L.; Castillo-Michel, H.; de la Torre-Roche, R.; Hawthorne, J.; Hernandez-Viezcas, J.A.; Loredo-Portales, R.; Majumdar, S.; Gardea-Torresday, J.; Dhankher, O.P.; White, J.C. Weathering in soil increases nanoparticle CuO bioaccumulation within a terrestrial food chain. Nanotoxicology 2017, **11**, 98–111

Figure Captions

Figure 1. (A) EXAFS and Fourier transform, (B) of studied samples and reference compounds. For each reference the average is on 2 scans, for the samples the average is on 8 scans.

Figure 2. Samples biomass. (A, B) Blue bars fresh weight, red bars dry weight. Different letters indicate significant differences among values according to Tukey's HSD test with $p<0.005$. (C) Samples water content. Different letters indicate significant differences among values according to Tukey's HSD test with $p<0.005$. (D) Samples Cadmium concentrations. The three asterisks indicate significant differences among groups of values according to Student's t-test with $p<0.005$. For all the analyses, each of the three biological replicates comprised 10 Petri dishes containing 25 plants.

Figure 3. XANES spectra of measured samples and model compounds. For each reference the average is on 2 scans, for the samples the average is on 8 scans.

Figure 4. Cd *K*-edge k^3-weighted EXAFS region (A) and Fourier transforms (B) of *at*-np01 grown on CdS QDs and $CdSO_4$. Solid lines are data, red lines are fits. For the samples the average is on 8 scans.

Figure 5. Schematic of the CdS QDs from uptake to detoxification within the plant cell. O= oxygen atoms, S= sulphur atoms, Cd^{2+} = Cd (II) ions, yellow circles= CdS QDs, yellow stars with thick border line= biotransformed CdS QDs; yellow stars with thin border line = bound particles left from the biotransformation. CdS QDs in the cell can be packaged into vesicles or be associated with several molecules, leading to their "biotransformation" into smaller, more reactive clusters, which do not retain the original QDs structure, and to the liberation of minor amounts of Cd (II) ions. The "biotransformed" nanostructures shows secondary bonds with S and O atoms within defense molecules produced as a consequence of the increased ROS production. Each phase can be explained through the utilization of different tools and approaches. Phase I, Exposure: 1, mutants are able to justify the different genetics mechanisms behind the physiological response between wt and tolerant phenotypes;[11] 2, measuring techniques for metals (FA-AAS, ICP-MS) are able to describe the intake of Cd.[11] Phase II, biotransformation: transition phase in which CdS QDs structure is modified to lower their reactivity. Phase III, detoxification: 3, XAS techniques allow to identify the changes in terms of biotransformation of the structure of CdS QDs and the Cd ions release, as described in the present work; 4-6, transcriptomics, proteomics, and metabolomics show the molecular follow up response related to the physico-chemical forms derived from the CdS QDs biotransformation.[11,59,61,69,70]

Tables

Table 1. EXAFS multiparameter fit details for studied samples and reference compounds

	k range (Å^{-1})	S_0^2	path	N	R (Å)	σ^2 (Å^{-2})
atnp01-CdS	3.0-12.0	0.79§	Cd-S	3.3(2)	2.483(2)	0.0069(6)
			Cd-O	0.5(1)	2.163(2)	0.000(1)
atnp01-CdSO$_4$	3.0-12.0	0.79§	Cd-S	2.1(5)	2.51(1)	0.006(2)
			Cd-O	2.6(2)	2.23(1)	0.008(2)
atnp02-CdS	3.0-12.0	0.79§	Cd-S	3.2(2)	2.488(2)	0.0056(4)
			Cd-O	0.5(1)	2.168(2)	0.000(1)
atnp02-CdSO$_4$	3.0-12.0	0.79§	Cd-S	2.2(6)	2.50(1)	0.005(2)
			Cd-O	2.2(5)	2.22(1)	0.006(2)
wt-CdS	3.0-12.0	0.79§	Cd-S	3.5(2)	2.483(2)	0.0061(6)
			Cd-O	0.4(2)	2.154(2)	0.000(2)
wt-CdSO$_4$	3.0-12.0	0.79§	Cd-S	2.3(8)	2.50(2)	0.005(3)
			Cd-O	2.3(7)	2.22(1)	0.007(3)
CdSO$_4$	3.0-9.5	0.74(5)	Cd-O	6	2.264(7)	0.0078(9)
CdS QDs	3.0-15.0	0.79(3)	Cd-S	4	2.518(3)	0.0061(4)

Notes: S_0^2= Many-body amplitude reduction factor (§fixed on the base of CdS QDs), N=path degeneracy, R=path length, σ^2=Debye-Waller factor. Note that EXAFS analysis cannot discriminate between atoms with similar Z such as N and O.

Table 2. Bond-valence strengths (v.u.) for Cd in the studied samples

	bond	***v***	***Σ v***	***N§***
atnp01-CdS	Cd-O	0.46	2.14	3.5
	Cd-S	0.58		
atnp01-CdSO$_4$	Cd-O	0.38	2.12	4.4

	Cd-S	0.54		
atnp02-CdS	Cd-O	0.45	2.05	3.6
	Cd-S	0.57		
atnp02-$CdSO_4$	Cd-O	0.39	2.07	4.3
	Cd-S	0.55		
wt-CdS	Cd-O	0.47	2.22	3.5
	Cd-S	0.58		
wt-$CdSO_4$	Cd-O	0.39	2.16	4.3
	Cd-S	0.55		
CdS	Cd-S	0.52	2.08	3.9
$CdSO_4$	Cd-O	0.33	1.98	6.1

Notes: B.V. parameters from Palenik (2006).[30] $N^{\S}$ is the ideal coordination number required to neutralize Cd charge, calculated using the Cd-S/Cd-O ratio derived from the EXAFS analysis. Estimated uncertainty on bond valence is 0.02 v.u.

Table 3. Cd-S/O distances similar to those of the studied samples

Cd coordination	<Cd-S> (Å)	<Cd-O> (Å)	References (n.)
CdS_2O_2	2.512	2.203	Beheshti et al., 2007 (38)
	2.508	2.250	Zhang et al., 1999 (36)
	2.493	2.231	Zhang et al., 2000 (37)
CdS_3O	2.515	2.245	Zhang et al., 2012 (34)
	2.519	2.229	Xu et al., 2015 (35)
CdS_2O_2	2.488	2.171	Phillips et al., 1995 (39)

Data from the Cambridge Crystallographic Data Centre (CCDC).

Table 4. Comparison between plant species showing similar Cd local environment

Compound/Species	<Cd-S> (Å)	N	<Cd-O> (Å)	N	References (n.)
A.halleri leaf	2.52–2.53	6.1	2.30–2.31	1.1	Huguet et al., 2012 (33)
Salsola kali leaf	2.52	1.0	2.14	1.0	Del a Rosa et al., 2004 (43)
Salsola kali stem	2.50	1.0	2.22	1.0	De la Rosa et al., 2004 (43)
N. cearulescens mature leaf	2.46	1.4	2.31	4.6	Kupper et al., 2004 (49)
T. praecox shoot	2.51	1.5 (7)	2.24	3.0 (8)	Vogel-Mikuš et al., 2010 (50)
Z. fabago leaf	2.48(1)	3.4 (5)	2.19(1)	2.2 (5)	Lefèvre et al., 2014 (47)
Z. fabago roots	2.48	3.4 (5)	2.19	1.0(5)	Lefèvre et al., 2016 (48)
A. halleri leaf	2.52	2.4	2.32	2.8	Isaure et al., 2015 (51)

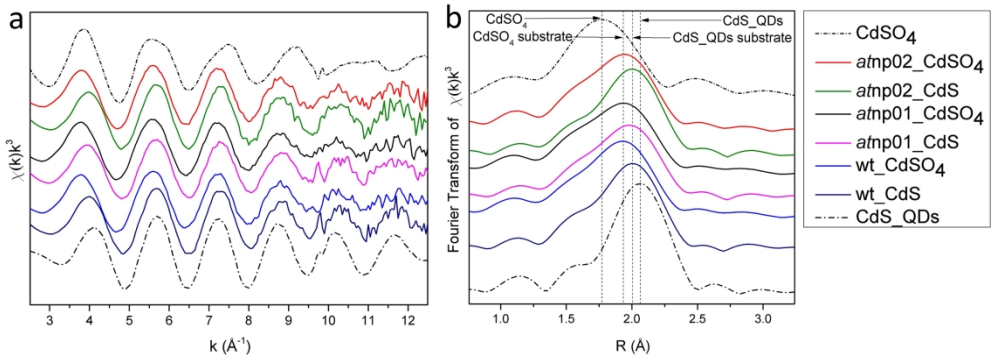

Figure 1. (A) EXAFS and Fourier transform, (B) of studied samples and reference compounds. For each reference the average is on 2 scans, for the samples the average is on 8 scans.

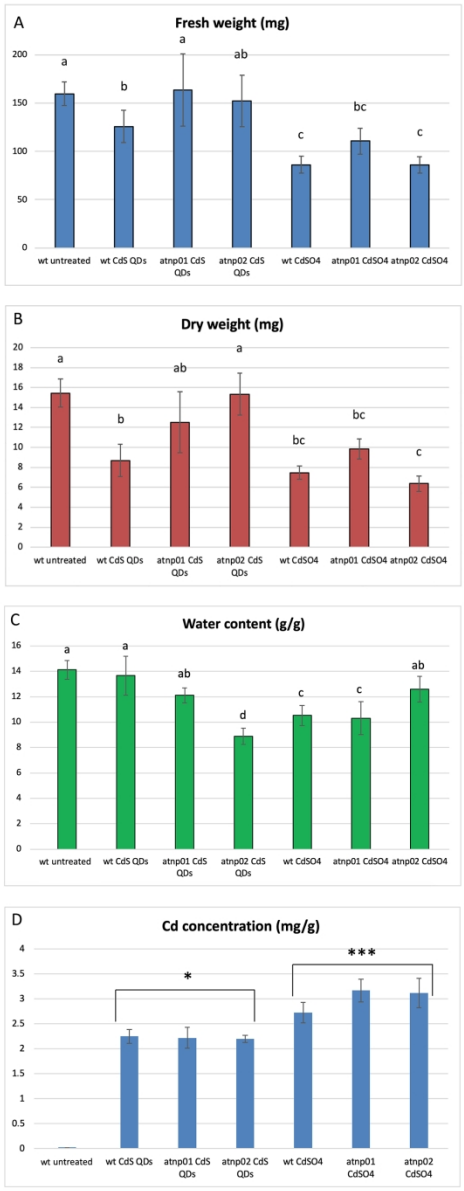

Figure 2. Samples biomass. (A, B) Blue bars fresh weight, red bars dry weight. Different letters indicate significant differences among values according to Tukey's HSD test with $p<0.005$. (C) Samples water content. Different letters indicate significant differences among values according to Tukey's HSD test with $p<0.005$. (D) Samples Cadmium concentrations. The three asterisks indicate significant differences among groups of values according to Student's t-test with $p<0.005$. For all the analyses, each of the three biological replicates comprised 10 Petri dishes containing 25 plants.

217x556mm (144 x 144 DPI)

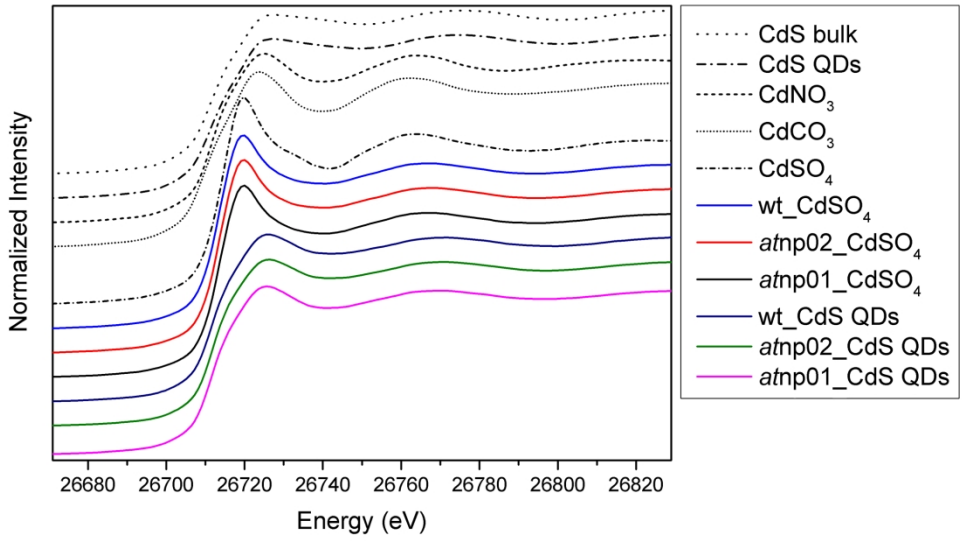

Figure 3. XANES spectra of measured samples and model compounds. For each reference the average is on 2 scans, for the samples the average is on 8 scans.

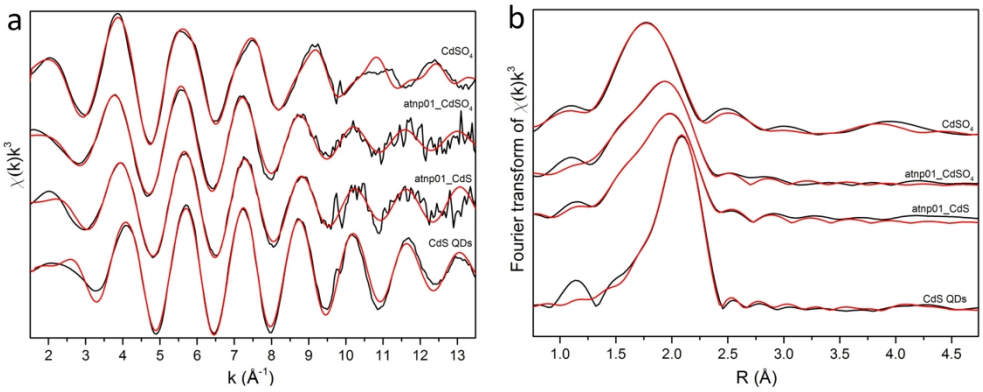

Figure 4. Cd K-edge k3-weighted EXAFS region (A) and Fourier transforms (B) of at-np01 grown on CdS QDs and CdSO4. Solid lines are data, red lines are fits. For the samples the average is on 8 scans.

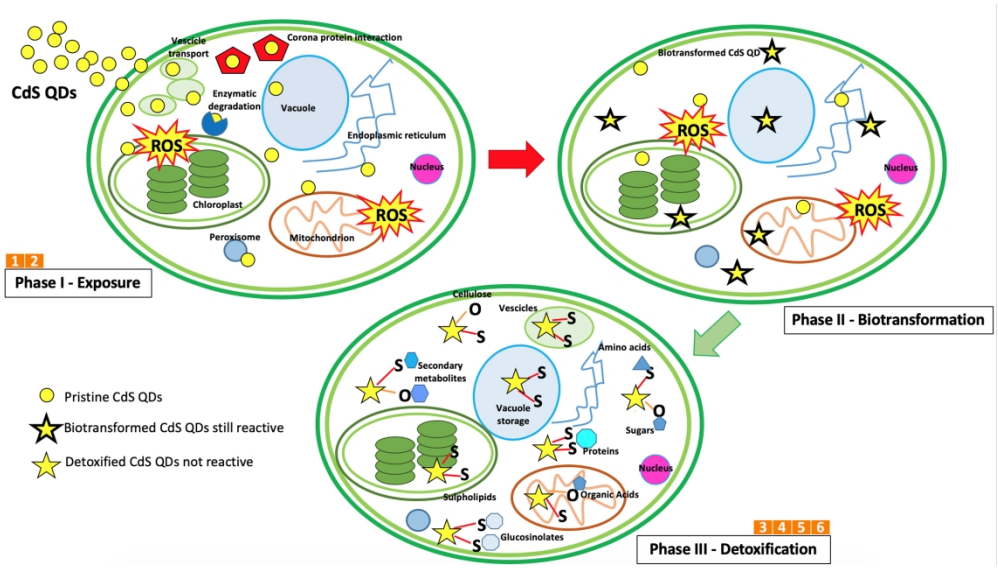

Figure 5. Schematic of the CdS QDs from uptake to detoxification within the plant cell. O= oxygen atoms, S= sulphur atoms, Cd 2+ = Cd (II) ions, yellow circles= CdS QDs, yellow stars with thick border line= biotransformed CdS QDs; yellow stars with thin border line = bound particles left from the biotransformation. CdS QDs in the cell can be packaged into vesicles or be associated with several molecules, leading to their "biotransformation" into smaller, more reactive clusters, which do not retain the original QDs structure, and to the liberation of minor amounts of Cd (II) ions. The "biotransformed" nanostructures shows secondary bonds with S and O atoms within defense molecules produced as a consequence of the increased ROS production. Each phase can be explained through the utilization of different tools and approaches. Phase I, Exposure: 1, mutants are able to justify the different genetics mechanisms behind the physiological response between wt and tolerant phenotypes;11 2, measuring techniques for metals (FA-AAS, ICP-MS) are able to describe the intake of Cd.11 Phase II, biotransformation: transition phase in which CdS QDs structure is modified to lower their reactivity. Phase III, detoxification: 3, XAS techniques allow to identify the changes in terms of biotransformation of the structure of CdS QDs and the Cd ions release, as described in the present work; 4-6, transcriptomics, proteomics, and metabolomics show the molecular follow up response related to the physico-chemical forms derived from the CdS QDs biotransformation.11,59,61,69,70

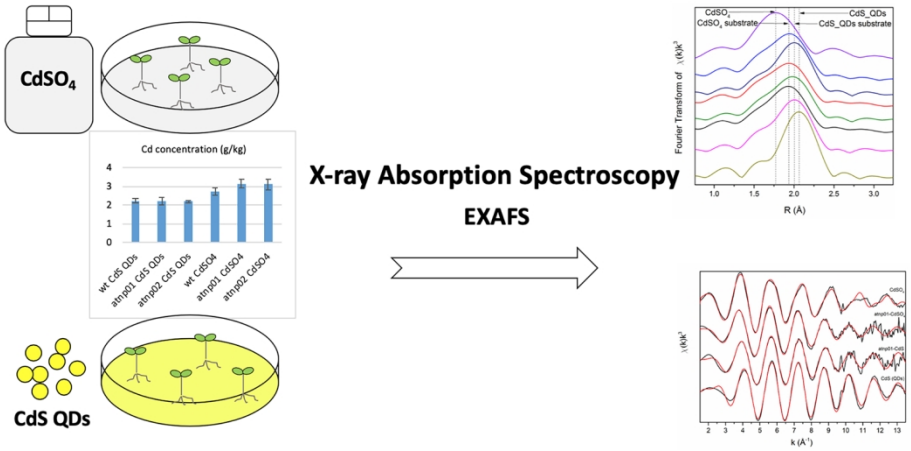
CdSO4
Cd concentration (g/kg)
wt CdS QDs
atmp01 CdS QDs
atmp02 CdS QDs
wt CdSO4
atmp01 CdSO4
atmp02 CdSO4
CdS QDs
X-ray Absorption Spectroscopy
EXAFS
CdS_QDs
CdS_QDs substrate
R (Å)
k (Å-1)